INVERSE SYNTHESIS OF ELECTROMAGNETIC MATERIALS USING HOMOGENIZATION BASED TOPOLOGY OPTIMIZATION

Y. El-Kahlout [†]

Istanbul Aydin University
Sefakoy, 34295 Kucukcekmece, Istanbul, Turkey

G. Kiziltas

Faculty of Engineering and Natural Sciences
Sabanci University
Orhanli, 34956 Tuzla, Istanbul, Turkey

Abstract—Recent studies on artificial materials demonstrate that substantial improvements in electromagnetic response can be attained by combining different materials subject to desired metrics. However, the perfect material combination is unique and extremely difficult to determine without automated synthesis schemes. In this paper, we develop a versatile approach to design the microstructure of periodic materials with prescribed dielectric and magnetic material tensors. The proposed framework is based on a robust material model and generalized inverse synthesis tool relying on topology optimization. The former is derived using homogenization theory and asymptotic expansion applied to Maxwell equations and can characterize the effects of anisotropy and loss of materials with periodic unit cells of arbitrary geometries and multi-phases much smaller than the wavelength. Resulting Partial Differential Equation (PDE) is solved numerically using Finite Element Analysis (FEA) and is validated with results in literature. The material model proves to be fast and numerically stable even with complex inclusions. The topology optimization problem is applied for the first time towards designing the unit cell topology of periodic electromagnetic materials from scratch with desired dielectric and magnetic tensors using off-the-shelf materials, i.e., readily available constituents obtained from

[†] Also with Sabanci University, Orhanli 34956, Tuzla, Istanbul, Turkey.

isotropic ceramic powders. The proposed framework's capability is demonstrated with five design examples. Design with anisotropic permittivity is also fabricated. Results show that the framework is capable of designing, in an automated fashion, non-intuitive material compositions from scratch with desired electromagnetic properties.

1. INTRODUCTION

Radio Frequency (RF) technologies are still mostly designed around properties of available materials. In achieving true design capability, however, the material itself need to be custom-designed for each application possibly for any desired electromagnetic property. Unusual properties of engineered artificial materials offer enormous potential for advanced applications in the millimeter wave [1], Terahertz [2] and optical frequency ranges [3]. Anisotropic ferrites, chiral materials, photonic crystals [4], left-handed [5–9] and non-reciprocal media [10] are well known paradigms. Strong controllability of dispersion in waveguides leads to compact and therefore cost efficient phase shifters and delay lines [11], miniaturized and enhanced integrated planar filter components [12], radiation molded frequency selective surfaces (FSS), e.g., for radomes, stealth planes, cellular phones [13, 14], sub wavelength imaging and diffraction applications [15, 16], and light emitting diodes coupling light generated in high refractive index materials into air effectively. As the variety of examples in the literature shows, the perfect combination of materials is unique and extremely difficult to determine without a formal approach [17–19]. Existing "conventional" metamaterials are based on analytical or experimental studies, i.e., a formal design approach to predict the exact spatial combination of material constituents from scratch does not exist. To a broader extent, the mostly intuitive or more recently simulation based design of materials with engineered permeability and permittivity, through carefully designed inclusions and the possible use of electronic components have been expanding through the decade [20–24]. Intuition of the expert designers at present is necessary for developing new devices as theory alone provides only basic designs. Nevertheless, this approach encounters difficulties such as the challenge to tune parameters and includes a lot of guesswork and more importantly is very time consuming. Therefore, the need for a systematic design methodology for developing advanced devices relying on unconventional material by designing their microstructure became very important. To address these issues, this paper presents for the first time, an inverse synthesis approach via the development of a generalized material model and its

integration to topology optimization for designing, in an automated fashion, the microstructure of novel magneto-dielectric materials from scratch. The material model is constructed by homogenizing Maxwell equations based on asymptotic expansion and therefore is an accurate tool for modeling materials with arbitrary geometry inclusions and multi-phases. The resulting effective material tensors of arbitrary materials are described by spatially varying periodic parameters and are numerically evaluated using the PDE-Coefficient Form module of COMSOL Multiphysics, which is a commercial analysis software based on the Finite Element Method. The other key module of the proposed design framework is the synthesis tool based on the powerful topology optimization method. The effective material model is linked through a Genetic Algorithm and Direct Search toolbox (GADS) to the topology optimization module which iteratively searches for the optimal unit cell topology of the periodic structure on a MATLAB interface. The objective of the topology optimization problem is to find the material distribution of the unit cell microstructure employing off-the-shelf isotropic constituents that delivers the desired constitutive material tensor. The paper is outlined as follows: After reviewing background related to both modules of the material synthesis framework, namely mathematical homogenization and topology optimization, detailed steps of the homogenization procedure of Maxwell equations are given. Then, the numerical evaluation of effective material tensors is explained in Section 3, where the derived formulas are numerically implemented for various unit cell configurations and validated with existing results in literature. The proposed material synthesis framework is presented next before demonstrating its use on five design examples where the goal is to achieve prescribed dielectric tensors by designing the microstructure topology of the dielectric material's unit cell. It is anticipated that advances in these research topics will allow, for the first time, integration of robust FEA based modeling tools and generalized design algorithms to generate automatically totally novel and yet unthinkable material designs that will lead to a new paradigm in electromagnetic design. The outcome of these investigations is anticipated to have also tremendous impact on materials based interdisciplinary research.

1.1. Homogenization Theory

Homogenization refers to replacing the inhomogeneous, periodic material in the microscopic scale with its homogeneous effective equivalent that has the same macroscopic effect as the original inhomogeneous structure [25–35]. The ability of computing the homogenized material property of such repetitive composites allows

replacing them with their equivalent homogenized constitutive material property such as the dielectric permittivity and magnetic permeability tensors, $\boldsymbol{\varepsilon}$ and $\boldsymbol{\mu}$. The effective process of homogenization of artificially engineered materials is only possible if the average lattice constant e or equivalently the dimension of the unit cell is electrically small enough ($e \prec\prec \lambda_g$, where λ_g is the guided wavelength). Otherwise, undesirable effects such as limited bandwidth, anisotropy, and poor refraction can take place [36].

The goal of assigning electromagnetic parameters to a composite or mixture of two or more component materials has long been the aim of traditional analytic homogenization theories, which have resulted in many well-known approximate mixing formulas, such as the Clausius-Mossotti, Maxwell-Garnett, or the coherent potential approximation [37], being the most popular ones. All known analytical methods, however, are valid under certain limitations and particular geometries or classes of structures.

S-parameter based homogenization is another homogenization technique that relies on retrieving the index of refraction ($n = n'+in''$) and the constitutive impedance ($z = z' + iz''$) or equivalently the effective constitutive parameters ($\varepsilon = n/z$ and $\mu = nz$) analytically via reflection and transmission coefficients calculated from Transfer Matrix simulations on a finite length of electromagnetic metamaterials. Smith et al. [38] implemented this method and showed that it gives an acceptable approximation but presents challenges in deciding upon the sign and branch of the solution for negative sign parameters (metamaterials). Improvement on this method was made later [39] and S-parameter numerical retrieval approaches for lossy bi-anisotropic media was introduced in [40]. Despite its versatility and ease of use, S-parameter retrieval approaches do not provide significant physical insight into the nature of the artificial material and the extracted reflection and transmission coefficients are not easily connected to analytical homogenization theories, which instead usually involve analysis of the local-field and current distributions.

Other homogenization methods have been developed over the years [41–44], but in general their scope of application is again limited to the static limit or to very specific geometries. With the advances in computing and analysis power, full wave simulations to solve Maxwell equations can be conducted, hence quantities such as local electric and magnetic fields, current distributions, and other quantities of interest can be found easily. These advances resulted in the emergence of purely numerical approaches to the homogenization of artificial structures avoiding the limitations associated with prior analytic homogenization models. One such technique based on averaging the local fields

obtained from a full-wave electromagnetic simulation or analytical calculation in order to determine the macroscopic fields was introduced in [31]. Once having computed the macroscopic fields, the method then determines the constitutive relationships between the macroscopic fields, arriving at the effective electromagnetic parameters. There is virtually no restriction on the contents of the unit cell, nor has the unit cell necessarily be small in comparison with the wavelength. Nevertheless, when the unit cell becomes more complicated by having multiple elements, additional bands are found in the eigenmode simulation making the analysis more difficult. Despite the difficulty, this procedure can be considered general and rigorous, but also suffers from important additional drawbacks. Namely, it relies on the solution of an eigenvalue problem solution and is not useful to retrieve the effective parameters either in frequency band-gaps or when the constituent materials have losses. Recently, another method was proposed to overcome these challenges in [29]. The proposed method formulated the homogenization problem as a source driven problem instead of relying on the solution of an eigenvalue problem and is therefore able to take into account effects of frequency dispersion, magneto-electric coupling, and spatial dispersion, even in frequency band-gaps where the propagation of electromagnetic waves is not allowed (band-gaps) or when the materials are lossy. However, the proposed method relies on the frequency dependent Maxwell Equations in a non-magnetic medium and therefore cannot be used to calculate the effective parameters of arbitrary periodic magnetic metamaterials.

An alternative approach to the homogenization of artificial structures avoiding the limitations associated with prior analytic homogenization models, similar to the 'averaging' concept proposed in [31], is the theory of a mathematical homogenization approach based on the asymptotic expansion also known as two-scale homogenization, which is a well established concept in the theory of partial differential equations with rapidly oscillating periodic coefficients [45]. Its main advantage is that the method is generalized enough and unlike analytical techniques, can handle unit cells with inclusions of arbitrary geometry and any number of phases with no additional computational cost. Also, instead of formulating the problem as an eigenvalue problem, two-scale homogenization works directly on the original form of the governing equations and is therefore able to result in expressions valid for effective constitutive tensors of both dielectric and magnetic materials, which can be lossy.

Another advantage of the mathematical homogenization approach is that it is generalized so that results apply to equations which arise in various different applications such as porous media, elastic

deformation, acoustics, material sciences, and heat conduction. The rigor of the approach has been justified with extensive mathematical theories including two-scale expansions, G-convergence, compensated compactness, and two-scale convergence [26, 37, 45–51]. More recently, many researchers have studied the application of two-scale homogenization to Maxwell equations. It was demonstrated that the macroscopic Maxwell equations can have significant differences when compared to their microscopic counterpart turning instantaneous material laws into constitutive laws with memory [26, 30, 47, 52–54]. A more general case was considered in [48] where polarization of the composite ingredient obeyed the Debye or Lorenz polarization laws with relaxation. Complexity of the macroscopic constitutive laws [55] and the structure of the macroscopic constitutive law was studied by focusing on the time-harmonic Maxwell equations [49, 56, 57]. As one of the pioneering work in the area of electromagnetic homogenization, the mathematical theory of homogenization was used to calculate the effective penetration depth in spatially periodic grids [58]. This, for the first time, was based on homogenizing Maxwell equations to obtain effective permittivity and permeability properties. The process relied on finding averaged parameters over a unit cell in the microscopic scale solving Maxwell equation via Finite Element Method. Homogenization theory was also applied to a 3D Bean's model for superconductivity. In this study, the electric field and the surface current over a "periodicity cell" with periodic boundary conditions was solved for iteratively to pass from local Bean's model to an increasingly larger space scale [59]. However, majority of existing homogenization studies based on asymptotic expansion do not involve numerical calculations, and their main result is a mathematical theorem which justifies the macroscopic harmonic Maxwell equations at a fixed low frequency. One of the few examples, which involves the numerical implementation is a study where asymptotic expansion based on the periodic unfolding method was used to extract the effective permittivity and effective conductivity based on the time-harmonic Maxwell equations. Their numerical evaluation was demonstrated at a fixed low frequency. Similarly, another study performed numerical evaluation of the parameters within the framework of the two-scale homogenization theory taking into account frequency dispersion [27]. In this paper, we further develop this research by applying the Finite Element Method to solve numerically the homogenization problem applying two-scale homogenization method formulated in [26, 45] to Maxwell equations and extract the effective parameters of periodic dielectric and magnetic materials, that can be in their most generalized form lossy and are made of inclusions with arbitrary shapes and multi-

phase material constituents. The numerical solution of the resulting PDE is carried out using a commercial FEA based solver, namely COMSOL Multiphysics, where the effective tensors are evaluated at a single frequency, for both isotropic and anisotropic effective material tensors with isotropic constituents. For the first time, the numerical material model based on two-scale homogenization is then used to synthesize the microstructure of electromagnetic material with desired material matrices using formal design techniques such as topology optimization.

The task of gathering information about the unit cell configuration from the effective parameters is basically known as inverse homogenization. In contrast to the significant amount of work addressing the theory of two-scale homogenization and quite a few focusing on the solution of the direct problem for a variety of different disciplines, there is limited work on inverse homogenization of electromagnetic materials. One major reason for this has been the lack of generalized and efficient inverse design tools that can be applied irrespectively of the application under consideration. Another reason for limited work on inverse homogenization is associated with lack of fabrication techniques capable of manufacturing dielectric and magnetic materials with complex spatial variation and multi-phase composition. Therefore, most metamaterial design studies today are conducted either by intuition or by varying only one or two design parameters. Cherkaev [60] applied inverse homogenization to evaluate the effective thermal or hydraulic conductivity of a random mixture of two different materials from the known effective complex permittivity of the same mixture. More specifically, measurements of the effective response of the random medium for a range of different parameters of the applied fields were used to reconstruct the geometric structural function of the mixture in the Stieltjes integral representation. This function was then used in predicting the thermal and hydraulic conductivity of the structure. In this paper, the aim is to address the inverse problem of constructing the topology of the unit cell using a formal and generalized synthesis tool instead of deferring information on an effective material parameter using information from another effective property. Towards that goal, topology optimization methods present us with an ideal tool, which has not been used towards exploring the full potential of artificial magneto-dielectrics for novel electromagnetic applications in literature. Its standard use and emergence in structural problems and its application as an inverse design tool for unique materials such as negative Poisson's ratio and negative thermal expansion coefficient [61, 62] were addressed for which related background is discussed in the next section.

1.2. Topology Optimization

Simply stated, design via topology optimization implies the determination of the best arrangement of material given a limited volume of available space within a given domain so as to obtain the optimal (electromagnetic) performance of the concept design [25]. The optimization process systematically and iteratively eliminates and re-distributes material throughout the domain to obtain a concept structure. An attractive aspect of topology optimization is that it transforms the design of geometry into a material distribution problem. When compared with more conventional size and shape optimization, where the topology of the device is assumed a priori and remains fixed, topology optimization offers much more freedom in design. Consequently, the possibility of topology design holds much greater promise because it dramatically increases the available design degrees of freedom. Originally developed within the Mechanical Engineering community for minimizing compliance, the field has expanded significantly, addressing many practical engineering problems including maximum stiffness, maximum eigenvalues, optimum compliant mechanisms or piezoelectric actuators and extreme material properties. Needless to mention it has been widely accepted in industry, with several commercial software packages incorporating such optimizations [63]. Comprehensive reviews on the mechanical, structural and computational aspects have been given in [64], the monographs by Bendsøe [65], Hassani and Hinton [66] and the review article by Rozvany [67]. The mathematical aspects of the concept are provided in [66].

More recently, the method was applied to electrostatic applications, photonic crystals and antenna design problems [25]. Topology optimization was originally introduced to the electromagnetic (EM) community using the Solid Isotropic Material with Penalization (SIMP) [68] to design a jumping ring. Over the years, the application area of topology optimization in EM was expanded from magneto-static [57] or eddy current systems [58] to 3D linear electrostatic problems [59]. Similarly, topology optimization was also applied to non-static electromagnetic applications. Two such applications refer to the design of waveguide components and a low-loss planar photonic crystal waveguide bend [69, 70] using topology optimization. Kiziltas et al. [18] extended the study further by integrating topology optimization based on SIMP method to full wave Finite Element Boundary Integral, FE-BI analysis tools. Using topology optimization, a threefold bandwidth enhancement of a miniature microstrip patch antenna was achieved by designing the spatial distribution of its dielectric substrate. Similarly, broadband dielectric resonator antennas were designed using

finite-difference time-domain method as the analysis tool in a topology optimization procedure focusing again on the spatial variation of the dielectric material [71]. In other studies [69, 72], topology optimization method was used to design two dimensional periodic structures that suppress electromagnetic power flow. Improved performance was achieved by considering the optimization of the layout of two materials with different electric permittivity over the design domain.

In conclusion, literature reports only few applications of topology optimization to non-static applications in electromagnetics [18, 69, 73]. Moreover, all existing studies on the topic are strictly focusing on the performance enhancement of the device through designing the material substrate instead of directly focusing on the design of the material itself. The effort of targeting the material itself or specifically the topology of its microstructure is by definition an inverse problem [74]. The solution of inverse problems is done iteratively. Historically, these iterations were carried out by cut and try operations taking months for each iteration or test. As a result, the design process relied on experience and intuition and was impractical. Today an inverse problem can be solved, at least in principle, by means of numerical optimization of an objective function subject to prescribed constraints. Such inverse problems based on topology optimization are addressed in literature for non-electromagnetic materials with unique properties such as negative Poisson's ratio and thermal expansion coefficient [75]. In this paper, we propose to develop an inverse synthesis framework by integrating topology optimization with an effective material model based on two-scale homogenization of Maxwell equations suitable to design materials with unique electromagnetic properties.

2. HOMOGENIZATION OF MAXWELL EQUATIONS

The derivation of the homogenized constitutive parameters represented by the permittivity and permeability tensors of electromagnetic materials is summarized in this section using Maxwell equations and will serve as the material model in developing a formal synthesis framework suitable for designing materials with desired homogenized/effective material tensors, $\boldsymbol{\varepsilon}_{eff}$ and $\boldsymbol{\mu}_{eff}$. For more details the reader is referred to [26, 45]. Theoretically, the material model holds for the infinite wavelength limit but examples in literature [76] show that this method practically holds for $\lambda \geq 10e$, where e is the average lattice constant.

If we assign a coordinate system $\mathbf{x} = [\ X_1\ \ X_2\ \ X_3\ ]^T$ in $\mathbf{R^3}$ space to define the domain of the composite material $\boldsymbol{\sigma}$, then assuming periodicity, the domain can be regarded as a collection of parallelepiped

cells of identical dimensions eY_1, eY_2, and eY_3 where Y_1, Y_2, and Y_3 are the sides of the base cell in a local (microscopic) coordinate system $\mathbf{y} = [\begin{array}{ccc} Y_1 & Y_2 & Y_3 \end{array}]^T = \mathbf{x}/e$ and e is a small quantity representing the lattice constant or the unit cell dimension. Therefore, any dependency on $\mathbf{y}$ can be considered $\mathbf{y}$-periodic for a fixed $\mathbf{x}$ in the macroscopic level. Moreover, it is assumed that the form and composition of the base cell varies in a smooth way with the macroscopic variable $\mathbf{x}$.

We consider the boundary value problem associated with the equation

$$\text{rot}\,(\mathbf{a}^e \text{rot}\,(\mathbf{u}_e)) + \mathbf{a}_0^e \mathbf{u}_e = \mathbf{f} \text{ in } \boldsymbol{\sigma} \tag{1}$$

where $\mathbf{a}^e$ and $\mathbf{a}_0^e$ are 3×3 matrices representing the constitutive parameters that can vary with respect to space and frequency, rot is the curl operator and $\mathbf{f}$ is a vector representing the source term, and $\boldsymbol{\sigma}$ is the unit cell domain.

We will study the behavior of the vector variable $\mathbf{u}_e$ as e approaches zero. Let the operator working on the field quantity $\mathbf{u}_e$ called $\mathbf{A}^e$ be defined as follows

$$\mathbf{A}^e = \text{rot}\,(\mathbf{a}^e \text{rot}) + \mathbf{a}_0^e \tag{2}$$

Using the chain rule of differentiation for rewriting the operator $\mathbf{A}^e$ and expanding the field vector $\mathbf{u}$ asymptotically as,

$$\mathbf{u} = \mathbf{u}_0\,(\mathbf{x}, \mathbf{y}) + e^1 \mathbf{u}_1\,(\mathbf{x}, \mathbf{y}) + e^2 \mathbf{u}_2\,(\mathbf{x}, \mathbf{y}) + \ldots \tag{3}$$

in the given boundary value problem proves that $\mathbf{u}_0$ is a function of $\mathbf{x}$ alone and for simplicity is denoted by $\mathbf{u}$

$$\mathbf{u}_0 = \mathbf{u}_0\,(\mathbf{x}) = \mathbf{u} \tag{4}$$

resulting in the following relation:

$$\text{rot}_y \mathbf{a}^e\,(\text{rot}_y \mathbf{u}_1 + \text{rot}_x \mathbf{u}) = \mathbf{0} \tag{5}$$

Now, let us define a vector quantity $\mathbf{w}$ as:

$$\mathbf{w} = \mathbf{a}^e\,(\text{rot}_y \mathbf{u}_1 + \text{rot}_x \mathbf{u}) \tag{6}$$

Averaging $\mathbf{w}$ over the problem domain $\boldsymbol{\sigma}$, it becomes a function of $\mathbf{x}$ alone because of the $\mathbf{y}$-periodicity over the domain and can be written with the aid of the averaging operator $\mathbf{M}$ or equivalently $\tilde{\mathbf{w}}$ as

$$\mathbf{M}\,(\mathbf{w}) = \tilde{\mathbf{w}} = \tilde{\mathbf{w}}\,(\mathbf{x}) \tag{7}$$

Using (5), (6), (7) and noting that the rotation with respect to y for a function of x alone is zero it can be deduced that there exists a scalar function $\boldsymbol{\Psi}\,(\mathbf{x}, \mathbf{y})$ the gradient of which is equal to the quantity $\mathbf{w} - \tilde{\mathbf{w}}$ i.e., $\mathbf{w} - \tilde{\mathbf{w}} = -\text{grad}_y \boldsymbol{\Psi}\,(\mathbf{x}, \mathbf{y})$.

Hence, (6) leads to:

$$-\text{div}_y\left((\mathbf{a}^e)^{-1}\,\text{grad}_y\Psi\right) = -\text{div}_y\left((\mathbf{a}^e)^{-1}\,\tilde{\mathbf{w}}\right) \tag{8}$$

The solution of the last equation is crucial for calculating the effective parameters as will be shown later. The solution is simplified by introducing a field quantity parameter $\boldsymbol{\theta}$ according the following relation.

$$\Psi = \boldsymbol{\theta}\cdot\tilde{\mathbf{w}} \tag{9}$$

Equation (8) can be rewritten using the last relation as

$$-\text{div}_y\left((\mathbf{a}^e)^{-1}\,\text{grad}_y\theta^j\right) = -\text{div}_y\left((\mathbf{a}^e)^{-1}\,\mathbf{e}_j\right) \tag{10}$$

where $\mathbf{e}_j$ is an identity vector in the corresponding axis. Equation (10) is solved for each spatial dimension, i.e., for a three-dimensional problem, $j = 1, 2, 3$.

Using (9), $\mathbf{w}$ can be written as

$$\mathbf{w} = \left(\mathbf{I} - \text{grad}_y\boldsymbol{\theta}\right)\tilde{\mathbf{w}} \tag{11}$$

where $\text{grad}_y\boldsymbol{\theta}$ for a three-dimensional problem is defined as the following

$$\text{grad}_y\boldsymbol{\theta} = \begin{bmatrix} \theta^1_{,y_1} & \theta^2_{,y_1} & \theta^3_{,y_1} \\ \theta^1_{,y_2} & \theta^2_{,y_2} & \theta^3_{,y_2} \\ \theta^1_{,y_3} & \theta^2_{,y_3} & \theta^3_{,y_3} \end{bmatrix} \tag{12}$$

Averaging $(\mathbf{a}^e)^{-1}\mathbf{w}$ in (6) yields

$$\mathbf{M}\left((\mathbf{a}^e)^{-1}\mathbf{w}\right) = \text{rot}\,\mathbf{u} \tag{13}$$

Substituting (11) into the last equation gives:

$$\mathbf{M}\left((\mathbf{a}^e)^{-1}\left(\mathbf{I} - \text{grad}_y\boldsymbol{\theta}\right)\right)\tilde{\mathbf{w}} = \text{rot}\,\mathbf{u} \tag{14}$$

We will define a new operator denoting homogenization, $\mathbf{H}$ working on $(\mathbf{a}^e)^{-1}$ as follows

$$\mathbf{H}\left((\mathbf{a}^e)^{-1}\right) = \mathbf{M}\left((\mathbf{a}^e)^{-1}\left(\mathbf{I} - \text{grad}_y\boldsymbol{\theta}\right)\right) \tag{15}$$

And hence $\tilde{\mathbf{w}}$ in (14) can be written in terms of the $\mathbf{H}$ operator as

$$\tilde{\mathbf{w}} = \mathbf{H}\left((\mathbf{a}^e)^{-1}\right)^{-1}\text{rot}\,\mathbf{u} \tag{16}$$

When the last equation is compared with (6), we conclude that the operator $\mathbf{H}$ is the homogenization operator that yields the effective property as $\tilde{\mathbf{w}}$ and rot $\mathbf{u}$ in (16) are the average quantities of $\mathbf{w}$ and

$(\mathrm{rot}_y \mathbf{u}_1 + \mathrm{rot}_x \mathbf{u})$, respectively, in (6). Applying (14) on the operator $\mathbf{A}^e$ given by (2), we get the homogenized operator as follows:

$$\mathbf{H}\left(\mathbf{A}^e\right) = \mathrm{rot}\left(\mathbf{H}\left(\left(\mathbf{a}^e\right)^{-1}\right)^{-1}\mathrm{rot}\right) + \boldsymbol{\lambda} \tag{17}$$

According to Theorem 11.4 in [45], if the operator $\mathbf{a}_0^e$ is anisotropic which is a general case, the homogenized operator can be written as

$$\mathbf{H}\left(\mathbf{A}^e\right) = \mathrm{rot}\left(\mathbf{H}\left(\left(\mathbf{a}^e\right)^{-1}\right)^{-1}\mathrm{rot}\right) + \mathbf{H}\left(\mathbf{a}_0^e\right) \tag{18}$$

The wave equation is represented by

$$\mathrm{rot}\left(\boldsymbol{\mu}^{-1}\mathrm{rot}\left(\mathbf{E}\right)\right) - \omega^2 \boldsymbol{\varepsilon}\mathbf{E} = -j\omega\mathbf{J}_i \text{ in } \boldsymbol{\sigma} \tag{19}$$

where $\mathbf{E}$ and $\mathbf{J}_i$ are the electric field and the induced current, i.e., $\mathbf{u}$ and $\mathbf{f}$, respectively. In the above derivations when $(\mathbf{a}^e)^{-1}$ and $\mathbf{a}_0^e$ are replaced by the permeability and permittivity tensors $\boldsymbol{\mu}$ and $\boldsymbol{\varepsilon}$, respectively, the homogenized permittivity and permeability tensors can be finally obtained as follows:

$$\mathbf{H}\left(\boldsymbol{\mu}\right) = \mathbf{M}\left(\boldsymbol{\mu}\left(\mathbf{I} - \mathrm{grad}_y\boldsymbol{\theta}\right)\right) \tag{20}$$

$$\mathbf{H}\left(\boldsymbol{\varepsilon}\right) = \mathbf{M}\left(\boldsymbol{\varepsilon}\left(\mathbf{I} - \mathrm{grad}_y\boldsymbol{\theta}\right)\right) \tag{21}$$

3. NUMERICAL IMPLEMENTATION OF THE HOMOGENIZED MATERIAL MODEL

In this section we make use of the homogenized form of the permeability and the permittivity dyads given by (20) and (21) and numerically evaluate the effective properties at the macro-scale level. The operator $\mathbf{M}$ is a straightforward operator since it is simply a volumetric averaging operator. Nevertheless, the intermediate field $\boldsymbol{\theta}$ requires careful consideration because it requires the solution of a partial differential equation given by (10). Towards that goal, we employ a finite element based simulation environment using COMSOL Multiphysics and utilize its Coefficient Form module. The objective is to solve this boundary value problem that is periodic in $\boldsymbol{\theta}$ on the boundaries of the unit cell. Figure 1 shows a representative unit cell that is discretized into 9×9 discrete design cells filled with material phases of four different dielectric constants, namely $\varepsilon \in \{20, 70, 100, 140\}$.

The most general form of the PDE in the Coefficient Form module of COMSOL is given as:

$$\mathrm{div}\left(-\mathbf{c}\,\mathrm{grad}\,\mathbf{u} - \mathbf{a}\mathbf{u} + \mathbf{Y}\right) + \boldsymbol{\alpha}\mathbf{u} + \boldsymbol{\beta}\mathrm{grad}\,\mathbf{u} = \mathbf{f} \tag{22}$$
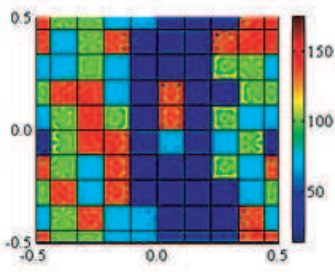
Figure 1. A typical two-dimensional periodic unit cell composed of four constituents with different permittivities $\varepsilon \in \{20, 70, 100, 140\}$ distributed discretely in a 9×9 cell configuration.
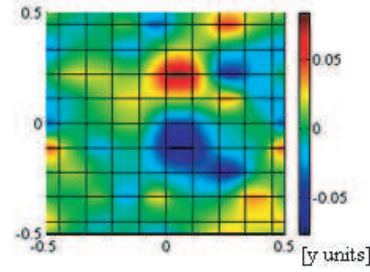

Figure 2. Intermediate θ^2 field distribution evaluated via Coefficient Form Module in COMSOL Multiphysics for material distribution of unit cell in Figure 1.

To transform the PDE to be solved for in (10) into the given form in (30) $\boldsymbol{\alpha}$, $\boldsymbol{\beta}$, and $\mathbf{Y}$ are assigned to zero matrices and $\mathbf{c} = \boldsymbol{\varepsilon}$. This turns the coefficients of the PDE into discontinuous parameters at the boundaries of two adjacent constituents inside the unit cell. If the right hand side were $(\mathbf{a}^e)^{-1}\mathbf{e}_j$ instead of $-\mathrm{div}_y\left((\mathbf{a}^e)^{-1}\mathbf{e}_j\right)$, then implementing (10) for spatially varying $\mathbf{a}$ would automatically result in loading terms at jumps in $\mathbf{a}$ and hence it would not be necessary to further manipulate. However, the right hand side of the equation to be solved corresponds to the divergence of these discrete coefficients of $\mathbf{a}$ that are equivalent to Dirac delta functions at the constituents' boundaries with infinite values. The integral of the right hand side across a boundary equals the difference of the constituents' coefficients of the domains sharing that boundary. However, the Dirac delta distribution cannot be expressed as a function that COMSOL Multiphysics is able to calculate numerically. Therefore, this challenge is overcome by preserving the finite element method's weak formulation of the right hand side in its original form. The weak formulation is obtained by multiplying the partial differential equation by an approximate solution field, v, and manipulating it based on integration by parts over the solution domain. The right hand side of the weak formulation at the constituent boundaries is assigned the coefficient difference value $\boldsymbol{\Phi}$ multiplied by the approximate solution field v directly as in the following integral expression:

$$\int_{\boldsymbol{\sigma}} \delta v = \boldsymbol{\Phi} v \qquad (23)$$

Practically, we set the source term $\mathbf{f}$ on the right hand side of (22) to zero and assign the constituent boundaries with corresponding difference $\boldsymbol{\Phi}$, of the coefficients around the specified boundary.

Periodicity condition requires θ to be equal at opposite boundaries of the unit cell, which completes the boundary value unit cell problem defined in (10). Figure 2 depicts the evaluated intermediate θ field distribution for the material distribution of the unit cell given in Figure 1.

The field data is then post-processed in MATLAB and the homogenized constitutive parameter is solved using Equation (21). The homogenized permittivity tensor calculated for the unit cell example given in Figure 1 is equal to $\boldsymbol{\varepsilon}_{eff} = \begin{bmatrix} 46.28 & 0.22 \\ 0.23 & 69.19 \end{bmatrix}$.

The mesh used for the analysis of the unit cell structure shown in Figure 1 and Figure 2 is given below in Figure 3. A convergence study was performed in order to determine the optimum mesh size. Starting from a coarse mesh, 7 different discretizations as suggested by the refinement strategy of COMSOL were used in performing the convergence study. Each discretization is given a mesh case number and the performance was measured using the corresponding homogenized effective permittivity matrix 2-norm, the relative error and number of triangular elements as given in Table 1 for all mesh cases. Resulting convergence history in terms of relative error for all mesh cases is plotted in Figure 4.

The relative error between two successive meshing cases was calculated according to the following

$$Err\,(k) = \sum_{\substack{i\,=\,1,2 \\ j\,=\,1,2}} \left(\left(\boldsymbol{\varepsilon}_k^H\,(i,j) - \boldsymbol{\varepsilon}_{k+1}^H\,(i,j) \right) / \boldsymbol{\varepsilon}_k^H\,(i,j)\,/4 \right)^2 \times 100 \quad (24)$$

where k refers to the mesh case number and $k + 1$ is the mesh case number of the finer mesh used in the comparison. Indices i and j

Table 1. Number of mesh elements, second norm of effective matrix, and relative error between two successive cases.

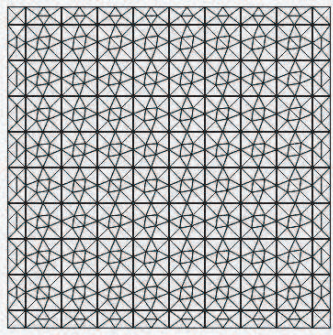| Case number (k)	1	2	3	4	5	6	7
Number of mesh elements	744	978	1058	1168	1271	2720	7968
$\left\| \boldsymbol{\varepsilon}_k^{\mathbf{H}} \right\|_2$	83.385	83.236	83.209	83.191	83.201	83.177	83.150
$Err\,(k)$	7.9394	1.9315	0.8261	0.1829	0.3876	0.3985	–

Figure 3. Discretization used for unit cell given in Figure 1 and Figure 2.
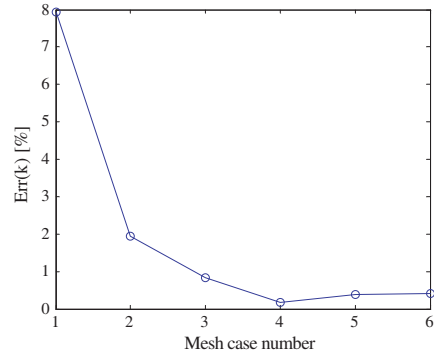
Figure 4. Relative error vs. Mesh Case Number (see Table 1) for the unit cell given in Figure 1 and Figure 2.

refer to the effective permittivity matrix row and column number, respectively. Case 4 with the corresponding discretization shown in Figure 4 was chosen as the optimal mesh size as the relative error dropped below 0.2% with 1168 elements. Therefore, this mesh is used for all the experiments when analyzing the performance of this unit cell structure with 9×9 design cell discretization throughout the paper.

4. VALIDATION OF THE HOMOGENIZED MATERIAL MODEL

The material model based on two-scale homogenization was introduced and implemented in previous sections. In this section, results of the proposed material model are compared with results obtained from analytical mixing formulas for different inclusions and unit cell configurations shown in Figure 6 and Figure 7.
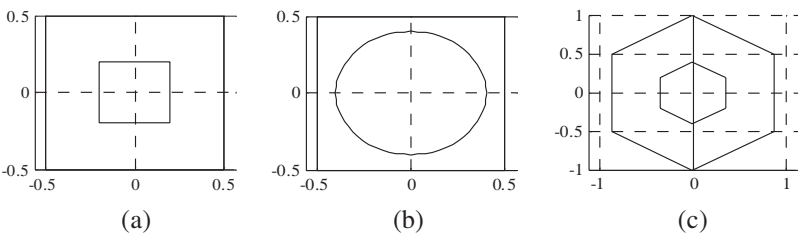
Figure 5 depicts a square shaped unit cell with (a) square and (b) circular inclusions, and (c) a honeycomb shaped unit cell with a honeycomb inclusion with a volume fraction of 0.4. The volume fraction is the ratio of the inclusion volume to the volume of the unit cell.

Results obtained using mixing formulas such as the Maxwell-Garnett and Bruggeman are depicted in Figure 6. Results belong to unit cells with a host and inclusion isotropic permittivity of 1 and 80, respectively. Figure 7 presents results for the same mixing formulas for unit cells with reverse host and inclusion permittivities. Simulations to obtain homogenized material model results were run at

a uniform volume fraction sampling with a stepsize of 0.025 ranging from a volume fraction of 0, i.e., no inclusion, to 1 with no host configuration for the square and the honeycomb cases, and from 0 to 0.775 volume fraction for the circular inclusion since higher volume fractions are geometrically not attainable for circular inclusions. A mesh convergence study similar to the one conducted in Section 3 yields 648, 688, 388 triangular mesh elements for the configurations shown in Figures 5(a), (b), and (c), respectively. As the results show, proposed material model shows a close behavior to the Maxwell-Garnet curve for all volume fractions.

As a second validation, the numerical implementation of the

(a)   (b)   (c)

Figure 5. A square shaped unit cell with (a) square and (b) circular inclusions, and (c) a honeycomb shaped unit cell with a honeycomb inclusion. Volume fraction of the inclusions is 0.4.
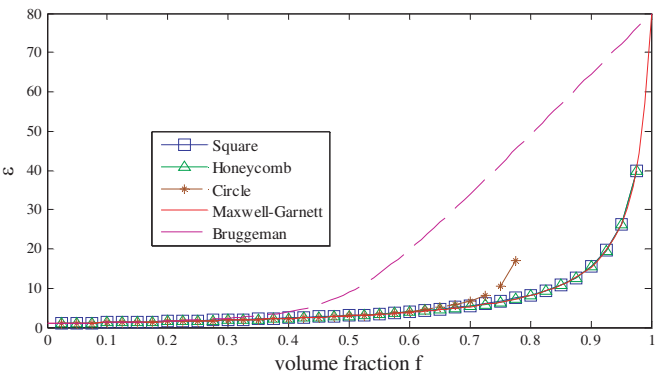

Figure 6. Effective dielectric constant vs. volume fraction of different inclusions in various unit cell configurations: Square in square, honeycomb in honeycomb and circles in square unit cells. Comparison is done with Maxwell Garnett, Bruggeman of host to inclusion ratio of 1-80.
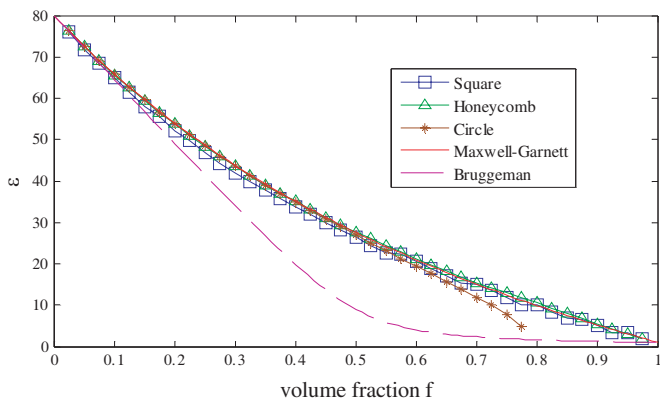
Figure 7. Effective dielectric constant vs. volume fraction of different inclusions in various unit cell configurations. Comparison is done with Maxwell Garnett, Bruggeman of host to inclusion ratio of 80-1.
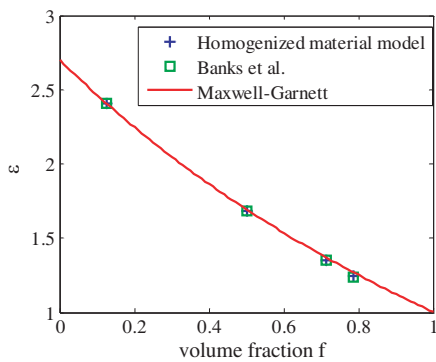

Figure 8. Comparison of proposed homogenized based method against model proposed by Banks et al. and Maxwell-Garnett formula.

material model is simulated with fabricated designs in literature. Figure 8 compares the proposed model with results in Banks et al. [48] for unit cell configurations with host and circular inclusion and dielectric constants of 2.7 and 1.003. Figure 9 compares results with results of Zouhdi et al. for unit cells with host and square inclusions and dielectric constants of 1 and 80, respectively. A perfect match of the results as observed for both comparisons proves the reliability of the homogenization based modeling tool.
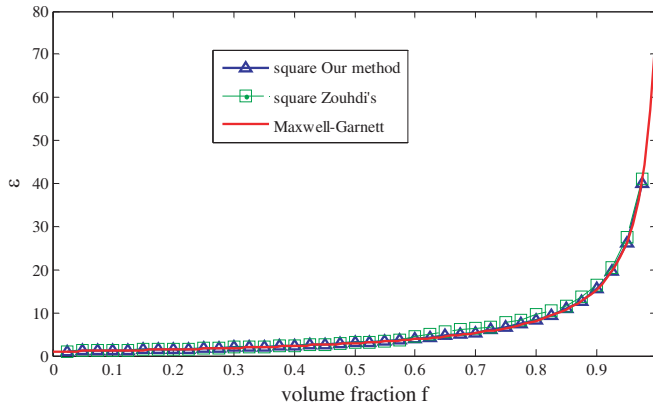
Figure 9. Comparison of proposed homogenized based method against model proposed by Zouhdi et al. and Maxwell-Garnett formula.

5. MATERIAL SYNTHESIS FRAMEWORK

The material synthesis framework is constructed by integrating the homogenized material model illustrated in the last section to a topology optimization design procedure. The flowchart of the material synthesis procedure is shown in Figure 10. The resulting topology optimization problem is solved using a genetic algorithm optimizer known as the Genetic Algorithm and Direct Search (GADS) toolbox available in MATLAB. We here choose GA mainly due to the simplicity of implementation. GA's are only practical if the computational time necessary for analysis, hence the time for the design study to converge to an optimum is acceptable for practical purposes. We acknowledge that GA's typically require a very large number of function evaluations but find that the computing time is acceptable for the design cases presented here.

Regarding the choice of material constituents, four instead of two material constituents were chosen among available shades to ensure a more effective design search. More specifically, as the targeted material matrices get more and more complicated (such as anisotropic and lossy) it is natural that increased number of material constituents will allow for a more effective search towards the optimum in the design space. However, there is not always a need for more than two material shades but the availability of four material constituents and the capability to directly translate this capability to the design model should allow for a more effective search and deliver a manufacturable design. This could as well relate to a two material design. It will depend on the targeted
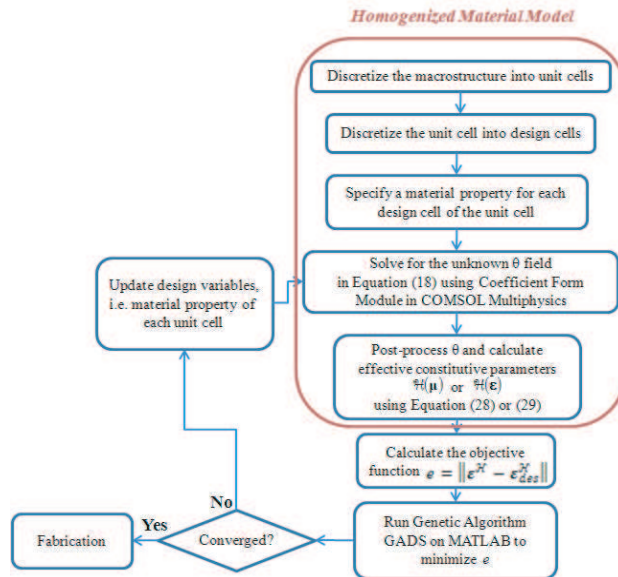
Figure 10. Material synthesis flowchart.

material property values and matrix structure where the resulting design could be as well comprised of two of the four available materials. It is also noted that in terms of manufacturing capability there is no additional challenge in producing a substrate with four vs. two ceramic constituents using the Dry Powder Deposition technique proposed in literature [77].

As a first step of the synthesis framework, the macrostructure, which essentially corresponds to the dielectric material substrate, is constructed using periodic repetition of the unit cells to be designed. These unit cells are then discretized into design cells (see Figure 1). A key aspect of the design method is that any structure or device, here the unit cell, not known a priori, is represented by specifying the material properties at every point of the fixed design domain. For electromagnetic applications, these are the permittivity and permeability values of the dielectric/magnetic material. In practice, to specify the material properties in the design region, the design space is discretized into material cells which are called design variable cells throughout the paper. These design variable cells are different from finite elements used in the analysis due to fabrication constraints dictated by the grid size of the mold shown in Figure 17(a), which is different from the finite element size constrained by the wavelength

in the electromagnetic material. Actually, the most straightforward image-based geometry representation is the "0/1" integer choice, where the design domain is represented by either a void or a filled/solid material and this was adopted in [78]. However, this formulation is not well-posed mathematically [79]. It can be well-posed by allowing for the design of materials with intermediate properties, which is also known as relaxation. Such a topology optimization model would be more suitable for the use of gradient based techniques. An example of a relaxed topology optimization model is SIMP [80], which allows for modeling of intermediate shades of the material but at the same time could drive the search for "0/1" type final designs using penalization and filtering techniques [25, 65]. Taking manufacturability constraints into account, design cells are assigned discrete permittivity values of available dielectric ceramics and act as the design variables of the problem, which are initially assigned to given values. Given the dielectric/magnetic material distribution of the unit cell, periodicity conditions are imposed and the next step is to solve for the θ field distribution based on the PDE in (10) using the Coefficient Form Module in COMSOL Multiphysics as described in Section 3. The resulting field distribution is subsequently post-processed by another in-house MATLAB program to solve for the effective material parameters described in (15). The task of the homogenized material model is completed (until the next iteration) by transferring the evaluated effective constitutive material tensors to the optimization module. The optimization module will then seek for an improved distribution of the dielectric/magnetic material property to achieve the targeted effective dielectric material tensor by minimizing an appropriate mathematical norm representing this objective.

A suitable objective function of the material synthesis problem corresponds to minimizing the error norm (e_{eff}) between the desired $\varepsilon_{des}^{\mathbf{H}}$ and calculated $\varepsilon^{\mathbf{H}}$ effective dielectric material tensors as

$$e_{eff} = \left\| \varepsilon^{\mathbf{H}} - \varepsilon_{des}^{\mathbf{H}} \right\| \tag{25}$$

The objective function at hand is a complex implicit function of the design variables, further justifying the choice of the optimization solver to be GA in order to effectively locate its minimum.

If the solver was chosen as a gradient based optimizer, which is known to converge to a local optimum evaluation of gradients would require the effective implementation of the adjoint sensitivity method. This analysis capability is not readily available in COMSOL, i.e., the ready to use sensitivity module available in COMSOL does not work on space dependent design variables such as the permittivity of each FE. In theory, the gradient information can be computed using the

adjoint method as was proposed and applied earlier to electromagnetic systems [18] and was applied to fluid-flow problems in a COMSOL environment [81]. It is noted that extra challenges rise when adopting the work in [81] to electromagnetic problems since quantities/fields of interest are frequency dependent and complex values and objectives functions (effective material matrices) are implicit functions of design variables, hence the adjoint sensitivity analysis obeys complex variable differentiation rules possibly taking also the frequency dependency into account.

The chosen Genetic Algorithm and Direct Search (GADS) toolbox here is available in MATLAB and includes routines for solving genetic optimization problems as well as other heuristic methods such as direct search and simulated annealing. The genetic algorithm is a method for solving optimization problems that is based on natural selection, the process that drives biological evolution. It is chosen here to solve the posed topology optimization problem. It repeatedly modifies a population of individual solutions, which correspond here to the microstructures of the dielectric topology. At each step, the genetic algorithm selects individuals at random from the current population to be parents and uses them to produce children for the next generation. Over successive generations, the population "evolves" toward an optimal solution. One can apply the genetic algorithm to solve a variety of optimization problems that are not well suited for standard optimization algorithms, including problems in which the objective function is discontinuous, non-differentiable, stochastic, or highly nonlinear where the design search typically takes much longer due to high number of generations needed for convergence. However, in the examples presented here, converged results using GA are obtained in less than a day leading to manufacturable designs in practical timespans despite the high number of generations. An optimization search in the material synthesis framework based on GADS is practically conducted by calling the function 'ga', which in its simplest form is a MATLAB statement given as follows:

$$[x \ fval] \ = ga(@fitnessfun, \ nvars, \ options) \qquad (26)$$

where @fitnessfun is the function to be minimized and corresponds to a MATLAB file which evaluates (25), nvars is the number of design variables and options is a structure that stores the genetic algorithm tuning parameters. The integration between the homogenized material module and the optimizer takes place via the fitness function in MATLAB. More specifically, the fitness function @fitnessfun calls a Matlab m-file that takes the design variable values from a predefined set that represent the constituents' constitutive parameters of the discretized design cells. The fitness function, then, prepares the

COMSOL model for the solution of (10) by updating the PDE coefficients $(\mathbf{a}^e)^{-1}$ and the weak form, $\boldsymbol{\Phi}$, given by (23), of the boundary conditions between the design cells of the right hand side of (10). These evaluations are repeated at each generation/iteration for each individual, i.e., for different material distributions of the unit cell until the optimization algorithm converges to an optimal material distribution that matches the desired effective material tensor. In the examples presented in this paper, the genetic algorithm numerically converges when the average change in the fitness value is less than a chosen tolerance value of 10^{-6}. To ensure an effective search within a diverse population, a number of optimization parameters need to be tuned. For the proposed material synthesis framework with chosen design cells with $9 \times 9 = 81$ design variables, a typical list and corresponding values of tuned genetic algorithm parameters are as follows: population size = 80; selection strategy function = remainder; scattered crossover function; scale parameter value = 0.75 and shrink mutation parameter value = 0.5.

6. VALIDATION AND DESIGN EXAMPLES

In this section five design examples are demonstrated including an initial sanity check which proves that the material synthesis framework indeed has the capabilities to design electromagnetic materials with both desired isotropic and anisotropic constitutive parameters from isotropic constituents. Although the proposed framework is based on a material model that can deal with both permittivity and permeability tensors, for fabrication purposes, the design examples presented in the next section focus only on the dielectric permittivity tensor. More specifically, a novel fabrication process capable of producing monolithic dielectric substrates made of spatially varying dielectrics was earlier proposed in [82]. This technique has been successfully employed to produce miniaturized antenna substrates using commercially available MCT ceramic powders with similar cofiring characteristics and low loss $(\tan(\delta) = 0.001)$. The dielectric constant values of available ceramic materials correspond to $\varepsilon \in \{20, 70, 100, 140\}$ and are chosen as the base dielectric phases to achieve desired dielectric non-lossy tensor matrices in the presented examples.

6.1. Design of Isotropic Dielectric Material Tensor with Homogeneous Phase

The isotropic design case presented here is intended to validate the design framework by targeting an isotropic permittivity $\boldsymbol{\varepsilon}_{des}^{\mathbf{H}} = 70$ using

two material shades of $\varepsilon \in \{20, 70\}$. The dielectric constituents chosen include the desired homogeneous phase itself, hence this example serves as a sanity check for the validity of the inverse synthesis framework. The unit cell is discretized into 20×20 design variable cells that will be occupied by the material constituents. By following the proposed material synthesis flowchart in Figure 10, the genetic algorithm converges to the correct naïve solution $\varepsilon^{\mathbf{H}} = 70$ in 357 generations. The genetic algorithm tuning parameters for the examples presented in this paper are shown in Table 2. Figure 11 depicts the convergence history of the GA optimization process for this example.

Table 2. Genetic algorithm tuning parameters of the substrate design examples.

		Design Example		
		Isotropic homogeneous	Isotropic inhomogeneous	Anisotropic
Population size		60	20	80
Elite count		2	2	2
Crossover fraction		0.9	0.9	0.9
Maximum generations		500	500	500
Selection function		remainder	remainder	remainder
Crossover function		scattered	scattered	scattered
Mutation func.	Scale	0.75	0.75	0.75
	Shrink	0.5	0.5	0.5

6.2. Design of Isotropic Dielectric Material Tensor with Inhomogeneous Phase

In the second design case conducted for the validation of the design framework, the same targeted isotropic permittivity of the first example, namely an $\varepsilon^{\mathbf{H}}_{des} = 70$ is desired using constituents with dielectric values $\varepsilon \in \{1, 100\}$, where this time the target phase dielectric constant of 70 is excluded. A mesh convergence study similar to the one in Section 3 applied on this new 20×20 design configuration yields 1600 triangular elements and is therefore chosen for both 20×20 design variable configurations in Figure 13 and Figure 15 below. For this example, the optimum design converged in 226 iterations as shown in the convergence history in Figure 12. The genetic algorithm tuning parameters used are given in Table 2. The objective function used in the optimization procedure according to relation (23) returns an error
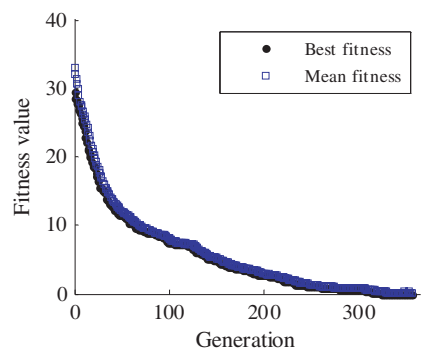
Figure 11. GA convergence history of a sanity check case of a unit cell with 20×20 design variable cells. Two material shades of $\varepsilon \in \{20, 70\}$ with a desired isotropic $\boldsymbol{\varepsilon}_{des}^{\mathbf{H}} = 70$ returns a homogeneous phase substrate of $\boldsymbol{\varepsilon}^{\mathbf{H}} = 70$.
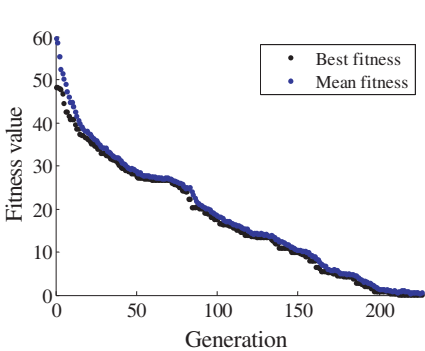
Figure 12. Genetic algorithm convergence history of a unit cell with 20×20 design variable cells: two material constituents with $\varepsilon \in \{1, 100\}$ and a desired isotropic dielectric value of $\boldsymbol{\varepsilon}_{des}^{\mathbf{H}} = 70$ returns a material tensor with $\boldsymbol{\varepsilon}^{\mathbf{H}} = \begin{bmatrix} 70.01 & -0.02 \\ -0.01 & 70.00 \end{bmatrix}$.
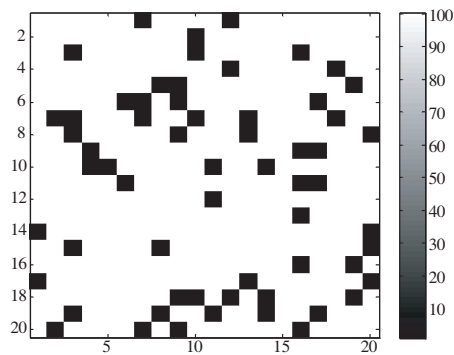

Figure 13. Resulting optimum material design of the example in Figure 12. Black and white shades are phases with dielectric constants 1 and 100, respectively.

norm of 0.020908 evaluated for the optimum design with a homogenized dielectric tensor of $\boldsymbol{\varepsilon}^{\mathbf{H}} = \begin{bmatrix} 70.01 & -0.02 \\ -0.01 & 70.00 \end{bmatrix}$. The resulting optimum material design distribution is shown in Figure 13. The volume fraction of the inclusion with $\varepsilon = 100$ returns a perfect match with the

Maxwell-Garnet mixture formula both predicting a value of 69.94 for the dielectric constant value.

6.3. Design of Anisotropic Dielectric Material Tensor

As a third example, an anisotropic dielectric material tensor is targeted and the material synthesis flowchart is followed in this validation example for a desired permittivity tensor of $\boldsymbol{\varepsilon}_{des}^{\mathbf{H}} = \begin{bmatrix} 45 & 0 \\ 0 & 70 \end{bmatrix}$.

The design unit cell in this example is discretized into 20×20 and 9×9 design variable cells. The design variables are selected from a subset of four material constituents with dielectric constant values of $\varepsilon \in \{20, 70, 100, 140\}$. The genetic algorithm returns an optimum effective dielectric material tensor of $\boldsymbol{\varepsilon}^{\mathbf{H}} = \begin{bmatrix} 45.52 & 0.00 \\ 0.03 & 69.47 \end{bmatrix}$ for the 20×20 design cells case and an error norm of 0.54. For the same targeted anisotropic dielectric tensor, the 9×9 discretized unit cell problem converged to an effective dielectric tensor of $\boldsymbol{\varepsilon}^{\mathbf{H}} = \begin{bmatrix} 45.11 & 0.09 \\ 0.10 & 69.88 \end{bmatrix}$ resulting in an error norm of 0.15 evaluated according to Equation (25). The convergence history for both problem solutions is depicted in Figure 14. As expected, the 9×9 configuration with 81 design variables converges faster than the 20×20 design configuration
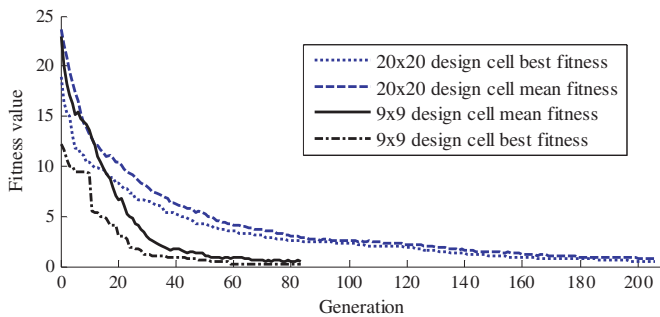

Figure 14. Genetic algorithm convergence history of a unit cell discretized with 20×20 and 9×9 design variable cells. Material constituents with $\varepsilon \in \{20, 70, 100, 140\}$ and a desired effective anisotropic dielectric tensor $\boldsymbol{\varepsilon}_{des}^{\mathbf{H}} = \begin{bmatrix} 45 & 0 \\ 0 & 70 \end{bmatrix}$ returns a homogenized substrate with $\boldsymbol{\varepsilon}^{\mathbf{H}} = \begin{bmatrix} 45.52 & 0.00 \\ 0.03 & 69.47 \end{bmatrix}$ and $\boldsymbol{\varepsilon}^{\mathbf{H}} = \begin{bmatrix} 45.11 & 0.09 \\ 0.10 & 69.88 \end{bmatrix}$ for the 20×20 and 9×9 design cells problems, respectively.
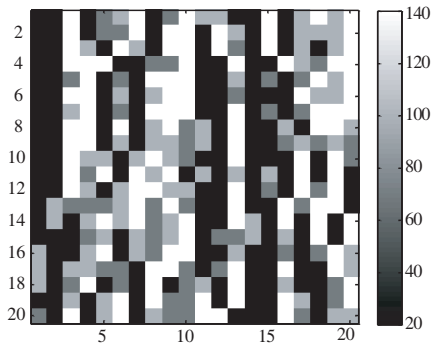
Figure 15. Optimal material distribution of the unit cell design with 20×20 design cells. The dielectric constants of the used constituents are 20, 70, 100, and 140.
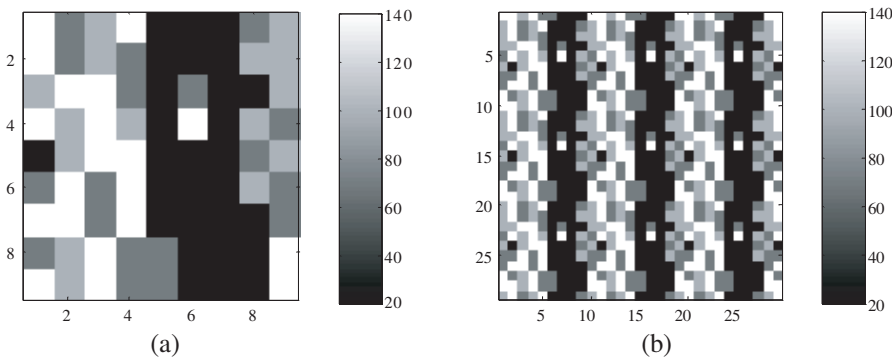

Figure 16. (a) Optimal material distribution of the unit cell design with 9×9 design cells and (b) a 3×3 array of the design unit cell to be fabricated.

with 400 design variable cells (84 vs. 206 generations, respectively) because it has less number of design variables and consequently spans much smaller design search space. Nevertheless, the small error norm of the optimum design of the 9×9 cell proves that this number of discrete cells is enough to fulfill the design target requirements. The optimum material design obtained using the 20×20 design cells is shown in Figure 15. The material distribution of the optimum design using the 9×9 design cells is shown in Figure 16(a) as a single unit cell and its 3×3 array configuration in Figure 16(b) that was also tested for manufacturability. More specifically, a 3×3 array configuration obtained using a repetition of the unit cell design resulting from the

(a) (b)

Figure 17. (a) Automated dispensing machine for DPD in action when depositing available ceramic powder constituents into desired material distribution for the 3×3 array of the unit cell discretized into 9×9 design variable configuration shown in Figure 16(a) resulting in (b) a desired deposited substrate.

first scheme is fabricated as shown in Figure 17 using Dry Powder Deposition (DPD) technique and commercial MCT ceramic powders (Trans-Tech Inc.) [77]. The resulting fabricated substrate in its pressed form is shown in Figure 16(b). Future work comprises using the substrate as part of a device design study such as an antenna design and testing the device upon which the substrate performance can be evaluated. It is finally noted that a relative convergence analysis for the homogenized dielectric constant matrices with different mesh sizes clearly indicates that the discretization employed in the analysis is enough and leads to reliable simulation results. Similar material topologies to the design example here with higher contrast material (with dielectric constituents of permittivity of 100 and 1) were obtained as a result of a previous design study for which simulations and experimental results agreed very well [18]. Therefore, designs obtained in this example with such a high-contrast material substrate and the discretization employed are expected to give reliable experimental results.

It is noted that the optimum number of triangular mesh elements used for the 9×9 discretization configuration is 1168 based on the convergence study conducted in Section 3 above.

6.4. Design of Anisotropic Dielectric Material Tensor with Non-zero Off-diagonal Terms

To demonstrate the ability of the proposed methodology to design dielectric tensors with off-diagonal elements a fourth design example

is conducted. In this example, the target is to design a material with an anisotropic material tensor that has the following parametric form.

$$\boldsymbol{\varepsilon} = \varepsilon_0 \begin{bmatrix} \varepsilon_a + \delta \cos 2\phi & \delta \sin 2\phi \\ \delta \sin 2\phi & \varepsilon_a - \delta \cos 2\phi \end{bmatrix} \tag{27}$$

where ϕ is the misalignment angle with the principal axes. Typical values of ε_a and δ are 125 and 40, respectively. This corresponds to a desired matrix value of $\boldsymbol{\varepsilon} = \begin{bmatrix} 159.64 & -20 \\ -20 & 90.36 \end{bmatrix}$ which basically represents a substrate with dielectric tensor value of $\boldsymbol{\varepsilon}$ rotated by 15 deg.

The design unit cell is discretized into 9×9 variable cells. The design variables are selected from a subset of four material shades with different dielectric constant values of $\varepsilon \in \{20, 70, 140, 240\}$. The optimization algorithm using the proposed material model converges when the average change in the fitness value is less than a set tolerance value of 10^{-6}. As a result, the application of the proposed synthesis framework returned an effective dielectric tensor of $\boldsymbol{\varepsilon}^{\mathbf{H}} = \begin{bmatrix} 155.80 & -14.68 \\ -14.74 & 94.24 \end{bmatrix}$ with an error norm of 6.5825. It is noted that the error norm (calculated according to (25)) of the 'optimal' design is relatively large. Hence, re-investigating the resulting design topologies given by Figure 18(a), the design cell size seems to be too large, i.e., the design domain is not well represented with the specified number of design cells, which needs to be increased in order to reach an optimal design. In order to overcome this problem, the number of
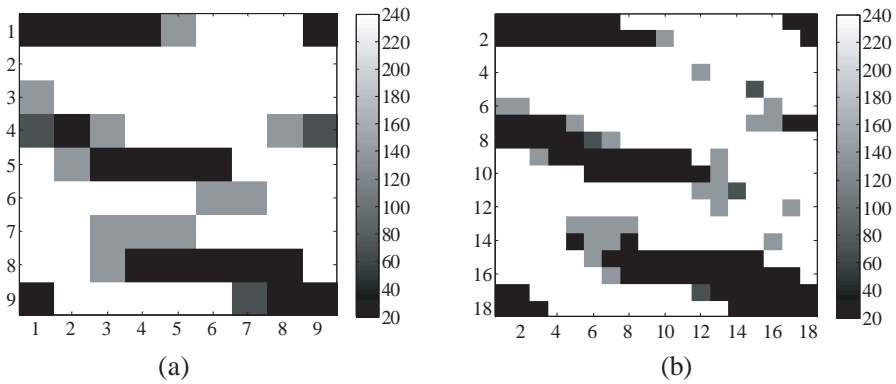

(a)

(b)

Figure 18. Optimal material distribution of the unit cell design using dielectric shades of $\varepsilon \in \{20, 70, 140, 240\}$ using (a) 9×9 design cells and (b) 18×18 design cells.
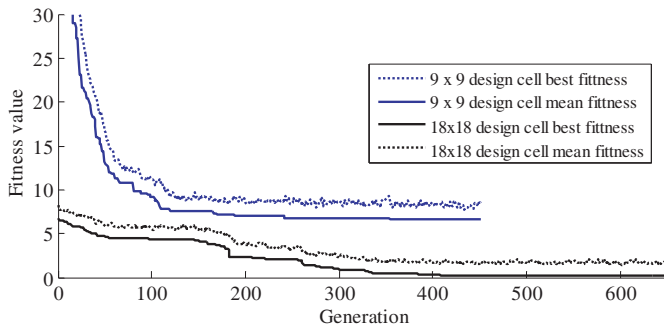
Figure 19. Genetic algorithm convergence history of the design with non-zero dielectric constant off-diagonal elements via 9×9 design cells (blue) and 18×18 design cells (black).

design cells was increased to 18×18 and the optimization process was restarted with its initial generation being the last generation of the earlier algorithm that resulted in the design shown in Figure 18(b). A mesh convergence study of this new 18×18 discretization configuration similar to that in Section 3 reveals an optimum value of 1296 triangular elements, which is used here. The optimum element number for the 9×9 case is 1168. The design with finer design cells converged to an effective dielectric tensor of $\boldsymbol{\varepsilon}^{\mathbf{H}} = \begin{bmatrix} 159.55 & -19.96 \\ -19.97 & 90.37 \end{bmatrix}$ with an error norm of 0.10. Convergence histories of both design cases are depicted in Figure 19.

6.5. Design of Anisotropic Dielectric Material Tensor with Loss

Another important feature of the proposed synthesis framework is its ability to handle loss. As a demonstration of this capability, a design example targeting a permittivity matrix with $\boldsymbol{\varepsilon} = \begin{bmatrix} 60 - j0.06 & 0 \\ 0 & 70 - j0.08 \end{bmatrix}$ is conducted using constituents with the following permittivity values: $\varepsilon \in \{ 20 - j0.012,\ 70 - j0.07,\ 100 - j0.120,\ 140 - j0.196 \}$. It is noted that the loss values are chosen to mimic expected behavior of available material for which a maximum loss tangent value of 0.001 is cited and the actual loss is expected to increase for the ceramic materials with increasing dielectric permittivity value. Use of the proposed synthesis framework resulted in an optimized material tensor with

$\varepsilon = \begin{bmatrix} 60.4817 - j0.0600 & 0.2825 - j0.0004 \\ 0.2489 - j0.0003 & 70.4191 - j0.0791 \end{bmatrix}$ where convergence was obtained in 51 generations tracing a convergence history shown in Figure 20. It is noted that the optimum number of the triangular mesh elements used here is 1168 elements as previously shown in Section 3 above. The resulting optimal material distribution for the unit cell is shown in Figure 21.
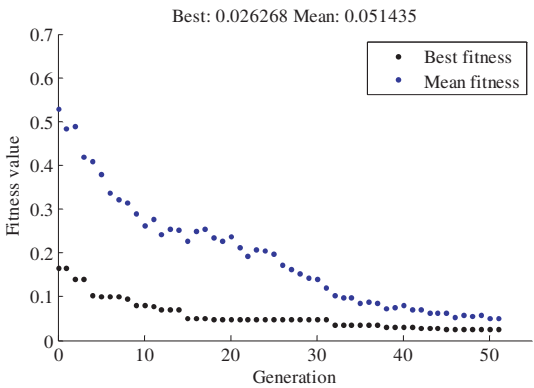

Figure 20. Genetic algorithm convergence history of the design with non-zero dielectric constant off-diagonal elements via 9×9 design cells.
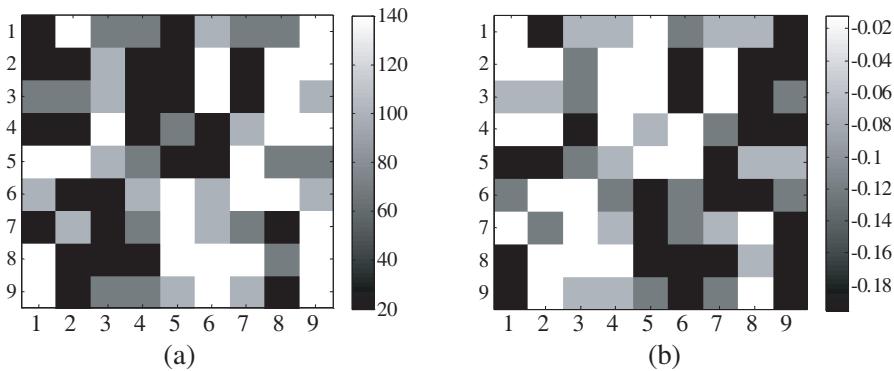

Figure 21. Optimal material distribution of the unit cell of the anisotropic lossy dielectric material tensor design using dielectric shades of $\varepsilon \in \{20 - j0.012, 70 - j0.07, 100 - j0.120, 140 - j0.196\}$ (a) ε' and (b) ε''.

7. CONCLUSIONS

A material synthesis framework based on topology optimization is proposed and applied for the first time towards designing the unit cell of periodic electromagnetic materials with desired dielectric tensors from readily available off-the-shelf constituents obtained from isotropic ceramic powders. The proposed framework is based on the integration of a robust effective material model derived using homogenization theory and asymptotic expansion applied to Maxwell equations. Therefore, it can characterize effects of anisotropy and loss in electromagnetic materials with periodic unit cells of arbitrary geometries and multi-phases much smaller than the wavelength. The numerical implementation of the effective material model at a specific frequency is conducted on a MATLAB interface using FEA based simulations in COMSOL Multiphysics for the solution of the resulting PDE. The results obtained for arbitrary geometries and material inclusions are validated with results from literature. The numerical implementation of the material synthesis framework is based on solving the topology optimization problem using GADS toolbox in MATLAB. To demonstrate the design capabilities of the proposed framework, it is applied to five design examples where periodic dielectric materials with desired isotropic anisotropic and lossy permittivity tensors are targeted. The resulting anisotropic material distribution is also fabricated to demonstrate its manufacturability. Results show that the homogenization technique integrated to topology optimization is able to design non-intuitive material compositions from scratch with desired electromagnetic dielectric properties. The validity and versatility of the proposed framework should allow for the automated synthesis of desired unique material properties for applications such as Magnetic Photonic Crystals, cloaking materials and left-handed media. By allowing for remarkable device performance improvements not possible via intuitive material designs, this capability is expected to make a significant impact in many critical applications including antennas, quasi-optical devices and beam formers.

REFERENCES

1. Shelby, R. A., D. R. Smith, and S. Schultz, "Experimental verification of a negative index of refraction," *Science*, Vol. 292, 77–79, Apr. 6, 2001.

2. Ferguson, B. and X. C. Zhang, "Materials for terahertz science and technology," *Nature Materials*, Vol. 1, 26–33, Sep. 2002.

3. Liu, N., H. C. Guo, L. W. Fu, S. Kaiser, H. Schweizer, and H. Giessen, "Three-dimensional photonic metamaterials at optical frequencies," *Nature Materials*, Vol. 7, 31–37, Jan. 2008.

4. Temelkuran, B., M. Bayindir, E. Ozbay, R. Biswas, M. M. Sigalas, G. Tuttle, and K. M. Ho, "Photonic crystal-based resonant antenna with a very high directivity," *Journal of Applied Physics,* Vol. 87, 603–605, Jan. 2000.

5. Ziolkowski, R. W. and E. Heyman, "Wave propagation in media having negative permittivity and permeability," *Physical Review E,* Vol. 64, 056625, 2001.

6. Baccarelli, P., P. Burghignoli, F. Frezza, A. Galli, P. Lampariello, G. Lovat, and S. Paulotto, "Fundamental modal properties of surface waves on metamaterial grounded slabs," *IEEE Transactions on Microwave Theory and Techniques,* Vol. 53, 1431–1442, 2005.

7. Ziolkowski, R. W. and A. D. Kipple, "Application of double negative materials to increase the power radiated by electrically small antennas," *IEEE Transactions on Antennas and Propagation,* Vol. 51, 2626–2640, Oct. 2003.

8. Tung, N. T., V. D. Lam, J. W. Park, M. H. Cho, J. Y. Rhee, W. H. Jang, and Y. P. Lee, "Single- and double-negative refractive indices of combined metamaterial structure," *Journal of Applied Physics,* Vol. 106, Sep. 2009.

9. Wu, B.-I., W. Wang, J. Pacheco, X. Chen, T. M. Grzegorczyk, and J. A. Kong, "A study of using metamaterials as antenna substrate to enhance gain," *Progress In Electromagnetics Research,* Vol. 51, 295–328, 2005.

10. Figotin, A. and I. Vitebskiy, "Electromagnetic unidirectionality in magnetic photonic crystals," *Physical Review B,* Vol. 67, 165210, 2003.

11. Perruisseau-Carrier, J. and A. K. Skrivervik, "Composite right/left-handed transmission line metamaterial phase shifters (mps) in mmic technology," *IEEE Transactions on Microwave Theory and Techniques,* Vol. 54, 1582–1589, 2006.

12. Ran, L., J. Huangfu, H. Chen, Y. Li, X. Zhang, K. Chen, and

J. A. Kong, "Microwave solid-state left-handed material with a broad bandwidth and an ultralow loss," *Physical Review B (Condensed Matter and Materials Physics),* Vol. 70, 073102-3, 2004.

13. Sungjoon, L., C. Caloz, and T. Itoh, "Metamaterial-based electronically controlled transmission-line structure as a novel leaky-wave antenna with tunable radiation angle and beamwidth," *IEEE Transactions on Microwave Theory and Techniques,* Vol. 52, 2678–2690, 2004.

14. Sungjoon, L., C. Caloz, and T. Itoh, "Metamaterial-based electronically controlled transmission-line structure as a novel leaky-wave antenna with tunable radiation angle and beamwidth," *IEEE Transactions on Microwave Theory and Techniques,* Vol. 53, 161–173, 2005.

15. Fang, N., H. Lee, C. Sun, and X. Zhang, "Sub–diffraction-limited optical imaging with a silver superlens," *Science,* 534–537, Apr. 22, 2005.

16. David, O. S. M., J. B. Richard, and R. W. Conrad, "Submicron imaging with a planar silver lens," *Applied Physics Letters,* Vol. 84, 4403–4405, 2004.

17. Jensen, J. S., O. Sigmund, L. H. Frandsen, P. I. Borel, A. Harpoth, and M. Kristensen, "Topology design and fabrication of an efficient double 90 photonic crystal waveguide bend," *IEEE Photonics Technology Letters,* Vol. 17, 1202–1204, 2005.

18. Kiziltas, G., D. Psychoudakis, J. L. Volakis, and N. Kikuchi, "Topology design optimization of dielectric substrates for bandwidth improvement of a patch antenna," *IEEE Transactions on Antennas and Propagation,* Vol. 51, 2732–2743, 2003.

19. Wang, S. and J. Kang, "Topology optimization of nonlinear magnetostatics," *IEEE Transactions on Magnetics,* Vol. 38, 1029–1032, 2002.

20. Wongkasemand, N., A. Akyurtlu, and K. A. Marx, "Group theory based design of isotropic negative refractive index metamaterials," *Progress In Electromagnetics Research,* Vol. 63, 295–310, 2006.

21. Thomas, Z., T. Grzegorczyk, B.-I. Wu, X. Chen, and J. A. Kong, "Design and measurement of a four-port device using metamaterials," *Optics Express,* Vol. 13, 4737–4744, Jun. 2005.

22. Marqués, R., J. Martel, F. Mesa, and F. Medina, "A new 2d isotropic left-handed metamaterial design: Theory and experiment," *Microwave and Optical Technology Letters,* Vol. 35, 405–408, 2002.

23. Shin, J., A. Akyurtlu, and M. Deshpande, "Comments on design, fabrication, and testing of double negative metamaterials," *IEEE Transactions on Antennas and Propagation,* Vol. 53, 891, 2005.

24. Sounas, D. L., N. V. Kantartzis, and T. D. Tsiboukis, "Focusing efficiency analysis and performance optimization of arbitrarily sized dng metamaterial slabs with losses," *IEEE Transactions on Microwave Theory and Techniques,* Vol. 54, 4111–4121, 2006.

25. Bendsøe, M. and O. Sigmund, *Topology optimization: Theory, Methods, and Applications*, Springer Verlag, 2003.

26. Sanchez-Palencia, E., *Non Homogeneous Media and Vibration Theory*, Springer-Verlag, Berlin, 1980.

27. Shelukhin, V. V. and S. A. Terentev, "Frequency dispersion of dielectric permittivity and electric conductivity of rocks via two-scale homogenization of the Maxwell equations," *Progress In Electromagnetics Research B,* Vol. 14, 175–202, 2009.

28. Baena, J. D., L. Jelinek, R. Marques, and M. Silveirinha, "Unified homogenization theory for magnetoinductive and electromagnetic waves in split-ring metamaterials," *Physical Review A (Atomic, Molecular, and Optical Physics),* Vol. 78, 013842, 2008.

29. Silveirinha, M. G., "Metamaterial homogenization approach with application to the characterization of microstructured composites with negative parameters," *Physical Review B,* Vol. 75, 115104, 2007.

30. Engstrom, C. and D. Sjoberg, "On two numerical methods for homogenization of Maxwell's equations," *Journal of Electromagnetic Waves and Applications,* Vol. 21, No. 13, 1845–1856, 2007.

31. Smith, D. R. and J. B. Pendry, "Homogenization of metamaterials by field averaging (invited paper)," *Journal of the Optical Society of America B-Optical Physics,* Vol. 23, 391–403, Mar. 2006.

32. Ouchetto, O., C. W. Qiu, S. Zouhdi, L. W. Li, and A. Razek, "Homogenization of 3-d periodic bianisotropic metamaterials," *IEEE Transactions on Microwave Theory and Techniques,* Vol. 54, 3893–3898, 2006.

33. Silveirinha, M. G. and C. A. Fernandes, "Homogenization of 3-d-connected and nonconnected wire metamaterials," *IEEE Transactions on Microwave Theory and Techniques,* Vol. 53, 1418–1430, 2005.

34. Ouchetto, O., S. Zouhdi, A. Bossavit, G. Griso, and B. Miara, "Homogenization of 3d structured composites of complex shaped inclusions," *PIERS Proceedings*, 22–26, Hangzhou, China, August 22–26, 2005.

35. Krokhin, A. A., P. Halevi, and J. Arriaga, "Long-wavelength limit (homogenization) for two-dimensional photonic crystals," *Physical Review B,* Vol. 65, 115208, 2002.

36. Caloz, C., A. Lai, and T. Itoh, "The challenge of homogenization in metamaterials," *New Journal of Physics,* Vol. 7, 15, Aug. 2005.

37. Sihvola, A., *Electromagnetic Mixing Formulas & Applications*, Institution of Electrical Engineers, London, UK, 1999.

38. Smith, D. R., S. Schultz, P. Markos, and C. M. Soukoulis, "Determination of effective permittivity and permeability of metamaterials from reflection and transmission coefficients," *Physical Review B,* Vol. 65, 195104, 2002.

39. Chen, X., T. M. Grzegorczyk, B.-I. Wu, J. J. Pacheco, and J. A. Kong, "Robust method to retrieve the constitutive effective parameters of metamaterials," *Physical Review E (Statistical, Nonlinear, and Soft Matter Physics),* Vol. 70, 016608-7, 2004.

40. Chen, X., B.-I. Wu, J. A. Kong, and T. M. Grzegorczyk, "Retrieval of the effective constitutive parameters of bianisotropic metamaterials," *Physical Review E,* Vol. 71, 046610, 2005.

41. Datta, S., C. T. Chan, K. M. Ho, and C. M. Soukoulis, "Effective dielectric constant of periodic composite structures," *Physical Review B,* Vol. 48, 14936, 1993.

42. Lamb, W., D. M. Wood, and N. W. Ashcroft, "Long wavelength electromagnetic propagation in heterogeneous media," *Physical Review B,* Vol. 21, 2248–2266, 1980.

43. Silveirinha, M. G., C. A. Fernandes, and J. R. Costa, "Electromagnetic characterization of textured surfaces formed by metallic pins," *IEEE Transactions on Antennas and Propagation,* Vol. 56, 405–415, Feb. 2008.

44. Pokrovsky, A. L. and A. L. Efros, "Electrodynamics of metallic photonic crystals and the problem of left-handed materials," *Physical Review Letters,* Vol. 89, 093901, 2002.

45. Bensoussan, A., J. L. Lions, and G. Papanicolaou, *Asymptotic Analysis of Periodic Structures*, Amsterdam, North-Holland, 1978.

46. Nguetseng, G., "A general convergence result for a functional related to the theory of homogenization," *SIAM Journal on Mathematical Analysis,* Vol. 20, 608–623, 1989.

47. Wellander, N. and S. Barbara, "Homogenization of the Maxwell equations: Case ii. Nonlinear conductivity," *Applications of Mathematics,* Vol. 47, 255–283, 2002.

48. Banks, H. T., V. A. Bokil, D. Cioranescu, N. L. Gibson, G. Griso,

and B. Miara, "Homogenization of periodically varying coefficients in electromagnetic materials," *Journal of Scientific Computing,* Vol. 28, 191–221, 2006.

49. Kristensson, G., "Homogenization of corrugated interfaces in electromagnetics," *Progress In Electromagnetics Research,* Vol. 55, 1–31, 2005.

50. Hashin, Z. and S. Shtrikman, "A variational approach to the theory of the effective magnetic permeability of multiphase materials," *Journal of Applied Physics,* Vol. 33, 3125–3131, 1962.

51. Jackson, J. D., *Classical Electrodynamics*, 2 Ed., John Wiley & Sons, New York, 1975.

52. Kristensson, G., "Homogenization of the Maxwell equations in an anisotropic material," *Radio Science,* Vol. 38, 8018, Apr. 2003.

53. Sjoberg, D., "Homogenization of dispersive material parameters for Maxwell's equations using a singular value decomposition," *Multiscale Modeling and Simulation,* Vol. 4, 760–789, 2006.

54. Wellander, N., "Homogenization of the Maxwell equations: Case i. Linear theory," *Applications of Mathematics,* Vol. 46, 29–51, 2001.

55. Huang, K. and X. Yang, "A method for calculating the effective permittivity of a mixture solution during a chemical reaction by experimental results," *Progress In Electromagnetics Research Letters,* Vol. 5, 99–107, 2008.

56. Ouchetto, O., S. Zouhdi, A. Bossavit, G. Griso, and B. Miara, "Modeling of 3-d periodic multiphase composites by homogenization," *IEEE Transactions on Microwave Theory and Techniques,* Vol. 54, 2615–2619, 2006.

57. Wellander, N. and G. Kristensson, "Homogenization of the Maxwell equations at fixed frequency," *SIAM Journal on Applied Mathematics,* Vol. 64, 170–195, 2003.

58. Bossavit, A., "Effective penetration depth in spatially periodic grids: A novel approach to homogenization," *EMC'94, International Symposium on Electromagnetic Compatibility*, 859–864, Dept. Elec. Engng., University La Sapienza, Roma, Italy, 1994.

59. Bossavit, A., "Superconductivity modelling: Homogenization of bean's model in three dimensions, and the problem of transverse conductivity," *IEEE Transactions on Magnetics,* Vol. 31, 1769–1774, 1995.

60. Cherkaev, E., "Inverse homogenization for evaluation of effective properties of a mixture," *Institute of Physics Publishing Inverse Problems,* Vol. 17, 1203–1218, Jun. 7, 2001.

61. Sigmund, O. and S. Torquato, "Design of materials with extreme thermal expansion using a three-phase topology optimization method," *Journal of the Mechanics and Physics of Solids,* Vol. 45, 1037–1067, 1997.

62. Sigmund, O., "A new class of extremal composites," *Journal of the Mechanics and Physics of Solids,* Vol. 48, 397–428, 2000.

63. Bloembaum, B., "The use of structural optimization in automotive design-state of the art and vision," presented at the WCSMO-3, Buffalo, 1999.

64. Bendsoe, M. P. and N. Kikuchi, "Generating optimal topologies in structural design using a homogenization method," *Computer Methods in Applied Mechanics and Engineering,* Vol. 71, 197–224, 1988.

65. Bendsøe, M., "Optimal shape design as a material distribution problem," *Structural and Multidisciplinary Optimization,* Vol. 1, 193–202, 1989.

66. Hassani, H. and E. Hinton, *Homogenization and Structural Topology Optimization Theory, Practice and Software*, Springer, Berlin, 1998.

67. Rozvany, G., "Aims, scope, methods, history and unified terminology of computer-aided topology optimization in structural mechanics," *Structural and Multidisciplinary Optimization,* Vol. 21, 90–108, 2001.

68. Dyck, D. N. and D. A. Lowther, "Automated design of magnetic devices by optimizing material distribution," *IEEE Transactions on Magnetics,* Vol. 32, 1188–1193, May 1996.

69. Jensen, J. S. and O. Sigmund, "Systematic design of photonic crystal structures using topology optimization: Low-loss waveguide bends," *Applied Physics Letters,* Vol. 84, 2022–2024, 2004.

70. Borel, P., A. Harpøth, L. Frandsen, M. Kristensen, P. Shi, J. Jensen, and O. Sigmund, "Topology optimization and fabrication of photonic crystal structures," *Opt. Express,* Vol. 12, 1996–2001, 2004.

71. Nomura, T., K. Sato, K. Taguchi, and T. Kashiwa, "Topology optimization method for antenna design using FDTD method," *IEICE Transactions on Electronics,* Vol. 12, 2196–2205, 2006.

72. Fuchi, K., A. R. Diaz, E. Rothwell, R. Ouedraogo, and A. Temme, "Topology optimization of periodic layouts of dielectric materials," *Structural and Multidisciplinary Optimization,* Vol. 42, 483–493, Jun. 2010.

73. Nomura, T., S. Nishiwaki, K. Sato, and K. Hirayama, "Topology

optimization for the design of periodic microstructures composed of electromagnetic materials," *Finite Elements in Analysis and Design,* Vol. 45, 210–226, February 2009.

74. Sigmund, O., "Materials with prescribed constitutive parameters: An inverse homogenization problem," *International Journal of Solids and Structures,* Vol. 31, 2313–2329, 1994.

75. Sigmund, O., "Systematic design of metamaterials by topology optimization," *Iutam Symposium on Modelling Nanomaterials and Nanosystems*, R. Pyrz and J. C. Rauhe (eds.), Vol. 13, 151–159, Springer, Netherlands, 2008.

76. Smith, D. R., D. C. Vier, N. Kroll, and S. Schultz, "Direct calculation of permeability and permittivity for a left-handed metamaterial," *Applied Physics Letters,* Vol. 77, 2246–2248, 2000.

77. Kiziltas, G. and Z. N. Wing, "Automated fabrication of three dimensional dielectric composites for RF applications," *IEEE Antennas and Propagation Society International Symposium and USNC/URSI National Radio Science*, Albuquerque, USA, 2006.

78. Li, Z., Y. Erdemli, J. Volakis, and P. Papalambros, "Design optimization of conformal antennas by integrating stochastic algorithms with the hybrid finite-element method," *IEEE Transactions on Antennas and Propagation,* Vol. 50, 676–684, 2002.

79. Sigmund, O., "Design of multi-physics actuators using topology optimization- part i: One material structures," *Computer Methods in Applied Mechanics and Engineering,* Vol. 190, 6577–6604, 2001.

80. Kiziltas, G., N. Kikuchi, J. Volakis, and J. Halloran, "Topology optimization of dielectric substrates for filters and antennas using simp," *Archives of Computational Methods in Engineering,* Vol. 11, 355–388, 2004.

81. Olesen, L. H., F. Okkels, and H. Bruus, "A high-level programming-language implementation of topology optimization applied to steady-state Navier-Stokes flow," *International Journal for Numerical Methods in Engineering,* Vol. 65, 975–1001, 2006.

82. Wing, Z. and J. Halloran, "Dry powder deposition and compaction for functionally graded ceramics," *Journal of the American Ceramic Society,* Vol. 89, 3406–3412, 2006.